

Data-Driven Control of Complex Networks

Giacomo Baggio

*Department of Information Engineering,
University of Padova, Padova, Italy*

Danielle S. Bassett

*Departments of Bioengineering, Physics & Astronomy,
Electrical & Systems Engineering, Neurology, and Psychiatry,
University of Pennsylvania, Philadelphia, USA
Santa Fe Institute, Santa Fe, USA*

Fabio Pasqualetti

*Department of Mechanical Engineering,
University of California at Riverside, Riverside, USA*
To whom correspondence should be addressed: fabiopas@engr.ucr.edu

(Dated: August 6, 2020)

Abstract

Our ability to manipulate the behavior of complex networks depends on the design of efficient control algorithms and, critically, on the availability of an accurate and tractable model of the network dynamics. While the design of control algorithms for network systems has seen notable advances in the past few years, knowledge of the network dynamics is a ubiquitous assumption that is difficult to satisfy in practice, especially when the network topology is large and, possibly, time-varying. In this paper we overcome this limitation, and develop a data-driven framework to control a complex dynamical network optimally and without requiring any knowledge of the network dynamics. Our optimal controls are constructed using a finite set of experimental data, where the unknown complex network is stimulated with arbitrary and possibly random inputs. In addition to optimality, we show that our data-driven formulas enjoy favorable computational and numerical properties even compared to their model-based counterpart. Although our controls are provably correct for networks with linear dynamics, we also characterize their performance against noisy experimental data and in the presence of nonlinear dynamics, as they arise when mitigating cascading failures in power-grid networks and when manipulating neural activity in brain networks.

I. INTRODUCTION

With the development of sensing, processing, and storing capabilities of modern sensors, massive volumes of information-rich data are now rapidly expanding in many physical and engineering domains, ranging from robotics [1], to biological [2, 3] and economic sciences [4]. Data are often dynamically generated by complex interconnected processes, and encode key information about the structure and operation of these networked phenomena. Examples include temporal recordings of functional activity in the human brain [5], phasor measurements of currents and voltages in the power distribution grid [6], and streams of traffic data in urban transportation networks [7]. When first-principle models are not conceivable, costly, or difficult to obtain, this unprecedented availability of data offers a great opportunity for scientists and practitioners to better understand, predict, and, ultimately, control the behavior of real-world complex networks.

Existing works on the controllability of complex networks have focused exclusively on a model-based setting [8–14], although, in practice, constructing accurate models of large-scale networks is a challenging, often unfeasible, task [15–17]. In fact, errors in the network model (i.e., missing or extra links, incorrect link weights) are unavoidable, especially if the network is identified from data (see, e.g., [18, 19] and Fig. 1(a)). This uncertainty is particularly important for network controllability, since, as exemplified in Fig. 1(b)-(c), the computation of model-based network controls tends to be unreliable and highly sensitive to model uncertainties, even for moderate size networks [20, 21]. It is therefore natural to ask whether network controls can be learned directly from data, and, if so, how well these data-driven control policies perform.

Data-driven control of dynamical systems has attracted increasing interest over the last few years, triggered by recent advances and successes in machine learning and artificial intelligence [22, 23]. The classic (indirect) approach to learn controls from data is to use a sequential system identification and control design procedure. That is, one first identifies a model of the system from the available data, and then computes the desired controls using the estimated model [24]. However, identification algorithms are sometimes inaccurate and time-consuming, and several direct data-driven methods have been proposed to bypass the identification step [25, Ch. III.10]. These include, among others, (model-free) reinforcement learning [26, 27], iterative learning control [28], adaptive and self-tuning control [29], and

behavior-based methods [30, 31].

The above techniques differ in the data generation procedure, class of system dynamics considered, and control objectives. In classic reinforcement learning settings, data are generated online and updated under the guidance of a policy evaluator or reward simulator, which in many applications is represented by an offline-trained (deep) neural network [32]. Iterative learning control is used to refine and optimize repetitive control tasks: data are recorded online during the execution of a task repeated multiple times, and employed to improve tracking accuracy from trial to trial. In adaptive control, the structure of the controller is fixed and a few control parameters are optimized using data collected on the fly. A widely known example is the auto-tuning of PID controllers [33]. Behavior-based techniques exploit a trajectory-based (or behavioral) representation of the system, and data that typically consist of a single, noiseless, and sufficiently long input-output system trajectory [31]. Each of the above data-driven approaches has its own limitations and merits, which strongly depend on the intended application area. However, a common feature of all these approaches is that they are tailored to or have been employed for closed-loop control tasks, such as stabilization or tracking, and not for finite-time point-to-point control tasks.

In this paper, we address the problem of learning from data point-to-point optimal controls for complex dynamical networks. Precisely, following recent literature on the controllability of complex networks [34, 35], we focus on control policies that optimally steer the state of (a subset of) network nodes from a given initial value to a desired final one within a finite time horizon. To derive analytic, interpretable results that capture the role of the network structure, we consider networks governed by linear dynamics, quadratic cost functions, and data consisting of a set of control experiments recorded offline. Importantly, experimental data are not required to be optimal, and can even be generated through random control experiments. In this setting, we establish closed-form expressions of optimal data-driven control policies to reach a desired target state and, in the case of noiseless data, characterize the minimum number of experiments needed to exactly reconstruct optimal control inputs. Further, we introduce suboptimal yet computationally simple data-driven expressions, and discuss the numerical and computational advantages of using our data-driven approach when compared to the classic model-based one. Finally, we illustrate with different numerical studies how our framework can be applied to restore the correct operation of power-grid networks after a fault, and to characterize the controllability properties of

functional brain networks.

While the focus of this paper is on designing optimal control inputs, the expressions derived in this work also provide an alternative, computationally reliable, and efficient way of analyzing the controllability properties of large network systems. This constitutes a significant contribution to the extensive literature on the model-based analysis of network controllability, where the limitations imposed by commonly used Gramian-based techniques limit the investigation to small and well-structured network topologies [20, 21].

II. RESULTS

A. Network dynamics and optimal point-to-point control

We consider networks governed by linear time-invariant dynamics

$$\begin{aligned} x(t+1) &= Ax(t) + Bu(t), \\ y(t) &= Cx(t), \end{aligned} \tag{1}$$

where $x(t) \in \mathbb{R}^n$, $u(t) \in \mathbb{R}^m$, and $y(t) \in \mathbb{R}^p$ denote, respectively, the state, input, and output of the network at time t . The matrix $A \in \mathbb{R}^{n \times n}$ describes the (directed and weighted) adjacency matrix of the network, and the matrices $B \in \mathbb{R}^{n \times m}$ and $C \in \mathbb{R}^{p \times n}$, respectively, are typically chosen to single out prescribed sets of input and output nodes of the network.

In this work, we are interested in designing open-loop control policies that steer the network output $y(t)$ from an initial value $y(0) = y_0$ to a desired one $y(T) = y_f$ in T steps. If y_f is output controllable [34, 36] (a standing assumption in this paper), then the latter problem admits a solution and, in fact, there are many ways to accomplish such a control task. Here, we assume that the network is initially relaxed ($x(0) = 0$), and we seek the control input $u_{0:T-1}^* = [u^*(T-1)^\top \dots u^*(0)^\top]^\top$ that drives the output of the network to y_f in T steps and, at the same time, minimizes a prescribed quadratic combination of the control effort and locality of the controlled trajectories.

Mathematically, we study and solve the following constrained minimization problem:

$$\begin{aligned} u_{0:T-1}^* &= \arg \min_{u_{0:T-1}} y_{1:T-1}^\top Q y_{1:T-1} + u_{0:T-1}^\top R u_{0:T-1} \\ &\text{s.t. (1) and } y_T = y_f, \end{aligned} \tag{2}$$

where $Q \succeq 0$ and $R \succ 0$ are tunable matrices¹ that penalize output deviation and input usage, respectively, and subscript $\cdot_{t_1:t_2}$ denotes the vector containing the samples of a trajectory in the time window $[t_1, t_2]$, $t_1 \leq t_2$ (if $t_1 = t_2$, we simply write \cdot_{t_1}). If $Q = 0$ and $R = I$, then $u_{0:T-1}^*$ coincides with the minimum-energy control to reach y_f in T steps [36].

Equation (2) admits a closed-form solution whose computation requires the exact knowledge of the network matrix A and suffers from numerical instabilities (Methods). In the following section, we address this limitation by deriving model-free and reliable expressions of $u_{0:T-1}^*$ that solely rely on experimental data collected during the network operation.

B. Learning optimal controls from non-optimal data

We assume that the network matrix A is unknown and that N control experiments have been performed with the dynamical network in (1). The i -th experiment consists of generating and applying the input sequence $u_{0:T-1}^{(i)}$, and measuring the resulting output trajectory $y_{0:T}^{(i)}$ (Fig. 2(a)). Here, as in, e.g., [37], we consider episodic experiments where the network state is reset to zero before running a new trial, and refer to the Supplement for an extension to the non-episodic setting and to the case of episodic experiments with non-zero initial state resets. We let $U_{0:T-1}$, $Y_{1:T-1}$, and Y_T denote the matrices containing, respectively, the experimental inputs, the output measurements in the time interval $[1, T-1]$, and the output measurements at time T . Namely,

$$\begin{aligned} U_{0:T-1} &= \begin{bmatrix} u_{0:T-1}^{(1)} & \cdots & u_{0:T-1}^{(N)} \end{bmatrix}, \\ Y_{1:T-1} &= \begin{bmatrix} y_{1:T-1}^{(1)} & \cdots & y_{1:T-1}^{(N)} \end{bmatrix}, \\ Y_T &= \begin{bmatrix} y_T^{(1)} & \cdots & y_T^{(N)} \end{bmatrix}. \end{aligned} \tag{3}$$

An important aspect of our analysis is that we do not require the input experiments to be optimal, in the sense of (2), nor do we investigate the problem of experiment design, i.e., generating data that are “informative” for our problem. In our setting, data are given, and these are generated from arbitrary, possibly random, or carefully chosen experiments.

By relying on the data matrices in (3), we derive the following data-driven solution to the minimization problem in (2) (see the Supplement):

$$\hat{u}_{0:T-1} = U_{0:T-1}(I - K_{Y_T}(LK_{Y_T})^\dagger L)Y_T^\dagger y_f, \tag{4}$$

¹ We let $A \succ (\succeq) 0$ denote a positive definite (semi-definite) matrix, and A^\top the transpose of A .

where L is any matrix satisfying $L^\top L = Y_{1:T-1}^\top Q Y_{1:T-1} + U_{0:T-1}^\top R U_{0:T-1}$, K_{Y_T} denotes a matrix whose columns form a basis of the kernel of Y_T , and the superscript symbol \cdot^\dagger stands for the Moore–Penrose pseudoinverse operation [38].

1. Minimum number of data to learn optimal controls

Finite data suffices to exactly reconstruct the optimal control input via the data-driven expression in (4) (see the Supplement). In Fig. 2(c), we illustrate this fact for the class of Erdős–Rényi networks of Fig. 2(b). Specifically, the data-driven input $\hat{u}_{0:T-1}$ equals the optimal one $u_{0:T-1}^*$ (for any target y_f) if the data matrices in (3) contain mT linearly independent experiments; that is, if $U_{0:T-1}$ is full row rank (Fig. 2(c), *left*). We stress that linear independence of the control experiments is a mild condition that is normally satisfied when the experiments are generated randomly. Further, if the number of independent trials is smaller than mT but larger than or equal to p , the data-driven control $\hat{u}_{0:T-1}$ still correctly steers the network output to y_f in T steps (Fig. 2(c), *right*), but with a cost that is typically larger than the optimal one. In this case, $\hat{u}_{0:T-1}$ is a suboptimal solution to (2), which becomes optimal (for any y_f) if the collected data contain p independent trials that are optimal as well.

2. Data-driven minimum-energy control

By letting $Q = 0$ and $R = I$ in (4), we recover a data-driven expression for the T -step minimum-energy control to reach y_f . We remark that the family of minimum-energy controls has been extensively employed to characterize the fundamental capabilities and limitations of controlling networks, e.g., see [9, 11, 14]. After some algebraic manipulations, the data-driven minimum-energy control input can be compactly rewritten as (see the Supplement)

$$\hat{u}_{0:T-1} = (Y_T U_{0:T-1}^\dagger)^\dagger y_f. \quad (5)$$

The latter expression relies on the final output measurements only (matrix Y_T) and, thus, it does not exploit the full output data (matrix $Y_{1:T-1}$). Equation (5) can be further approximated as

$$\hat{u}_{0:T-1} \approx U_{0:T-1} Y_T^\dagger y_f. \quad (6)$$

This is a simple, suboptimal data-based control sequence that correctly steers the network to y_f in T steps, as long as p independent data are available. Further, and more importantly, when the input data samples are drawn randomly and independently from a distribution with zero mean and finite variance, (6) converges to the minimum-energy control in the limit of infinite data (see the Supplement).

Fig. 3(a) compares the performance (in terms of control effort and error in the final state) of the two data-driven expressions (5) and (6), and the model-based control as a function of the data size N . While the data-driven control in (5) becomes optimal for a finite number of data (precisely, for $N = mT$), the approximate expression (6) tends to the optimal control only asymptotically in the number of data (Fig. 3(a), *left*). In both cases, the error in the final state goes to zero after collecting $N = p$ data (Fig. 3(a), *right*). For the approximate control (6), we also establish upper bounds on the size of the dataset to get a prescribed deviation from the optimal cost in the case of Gaussian noise. Our non-asymptotic analysis indicates that this deviation is proportional to the worst-case control energy required to reach a unit-norm target. This, in turn, implies that networks that are “easy” to control require fewer trials to attain a prescribed approximation error (see the Supplement).

3. Numerical and computational benefits of data-driven controls

By relying on the same set of experimental data, in Fig. 3(b), we compare the numerical accuracy, as measured by the error in the final state, of the data-driven controls (5) and (6) and the minimum-energy control computed via a standard two-step approach comprising a network identification step followed by model-based control design. First, we point out that if some nodes of the network are not accessible ($C \neq I$) and no prior information about the network structure is available, then it is impossible to exactly reconstruct the network matrix A using (any number of) data [39]. In contrast, the computation of minimum-energy inputs is always feasible via our data-driven expression, provided that enough data are collected. We thus focus on the case in which all nodes can be accessed ($C = I$). We consider Erdős–Rényi networks with n nodes as in Fig. 2(b) and we select $m = \lfloor n/10 \rfloor$ control nodes (forming matrix B). To reconstruct the network matrices A and B , the subspace-based identification technique described in Methods. Data-driven strategies significantly outperform the standard sequential approach for both dense (Fig. 3(b), *top*) and sparse

topologies (Fig. 3(b), *bottom*). This poor performance of the standard approach is somehow expected because, independently of the network identification procedure, the standard two-step approach requires a number of operations larger than those required by the data-driven approach, resulting in a potentially higher sensitivity to round-off errors. Also, it is interesting to note that the data-driven approach is especially effective for large, dense networks for which the standard approach leads to errors of considerable magnitude (up to approximately 10^2).

A further advantage in using data-driven controls over model-based ones arises when dealing with massive networks featuring a small fraction of input and output nodes. Specifically, in Fig. 3(c) we plot the time needed to numerically compute the data-driven and model-based controls as a function of the size of the network. We focus on Erdős–Rényi networks as in Fig. 2(b) of dimension $n \geq 1000$ with $\lfloor n/100 \rfloor$ input and output nodes and a control horizon $T = 50$. The model-based control input requires the computation of the first $T - 1$ powers of A (Methods). The computation of the data-driven expressions (5) and (6) involves, instead, linear-algebraic operations on two matrices ($U_{0:T-1}$ and Y_T) that are typically smaller than A when n is very large (precisely, when $T < n/m$ and $N < n$). Thus, the computation of the control input via the data-driven approach is normally faster than the classic model-based computation (Fig. 3(c), *left*). In particular, the data-driven control (6), although suboptimal, yields the most favorable performance due to its particularly simple expression. Finally, we note that the error in the final state committed by the data-driven controls is always upper bounded by 10^{-5} and thus it has a negligible effect on the control accuracy (Fig. 3(c), *right*).

4. *Data-driven controls with noisy data*

The analysis so far has focused on noiseless data. A natural question is how the data-driven controls behave in the case of noisy data. If the noise is unknown but small in magnitude, then the established data-driven expressions will deviate slightly from the correct values (see the Supplement). However, if some prior information on the noise is known, this information can be exploited to return more accurate control expressions. A particularly relevant case is when data are corrupted by additive i.i.d. noise with zero mean and known

variance.² Namely, the available data read as

$$\begin{aligned} U_{0:T-1} &= \bar{U}_{0:T-1} + \Delta_U, \\ Y_{1:T-1} &= \bar{Y}_{1:T-1} + \Delta_Y, \\ Y_T &= \bar{Y}_T + \Delta_{Y_T}, \end{aligned} \tag{7}$$

where $\bar{U}_{0:T-1}$, $\bar{Y}_{1:T-1}$, \bar{Y}_T denote the ground truth values and Δ_U , Δ_Y , and Δ_{Y_T} are random matrices with i.i.d. entries with zero mean and variance σ_U^2 , σ_Y^2 , and $\sigma_{Y_T}^2$, respectively. Note that the noise terms Δ_Y and Δ_{Y_T} may also include the contribution of process noise acting on the network dynamics. In this setting, it can be shown that the data-driven control (4) and the data-driven minimum-energy controls (5) and (6) are typically not consistent; that is, they do not converge to the true control inputs as the data size tends to infinity (see the Supplement for a concrete example). However, by suitably modifying these expressions, it is possible to recover asymptotically correct data-driven formulas (Supplement). The key idea is to add correction terms that compensate for the noise variance arising from the pseudoinverse operations. In particular, the asymptotically correct version of the data-driven controls (5) and (6) read, respectively, as

$$\hat{u}'_{0:T-1} = (Y_T U_{0:T-1}^\top (U_{0:T-1} U_{0:T-1}^\top - N\sigma_U^2 I)^\dagger)^\dagger y_f, \tag{8}$$

$$\hat{u}''_{0:T-1} = U_{0:T-1} Y_T^\top (Y_T Y_T^\top - N\sigma_{Y_T}^2 I)^\dagger y_f, \tag{9}$$

where we used the fact that $X^\dagger = X^\top (X X^\top)^\dagger$ for any matrix X [38], and $N\sigma_U^2 I$ and $N\sigma_{Y_T}^2 I$ represent the noise-dependent correction terms. Note, in particular, that if the noise corrupts the output data Y_T only, then (8) coincides with the original data-driven control (5), so that no correction is needed. Similarly, if the noise corrupts the input data U_T only, then (9) coincides with the data-driven control (6).

C. Applications

To demonstrate the potential relevance and applicability of the data-driven framework presented thus far, we present two applications of our data-driven control formulas.

² The different types of noise are assumed to be zero-mean to simplify the exposition. With slight modifications, non zero-mean noise could also be accommodated by our approach.

1. Data-driven fault recovery in power-grid networks

We address the problem of restoring the normal operation of a power-grid network after the occurrence of a fault which desynchronizes part of the grid. If not mitigated in a timely manner, such desynchronization instabilities may trigger cascading failures that can ultimately cause major blackouts and grid disruptions [40–42]. In our case study, we consider a line fault in the New England power grid network comprising 39 nodes (29 load nodes and 10 generator nodes), as depicted in Fig. 4(a), and we compute an optimal point-to-point control from data to recover the correct operation of the grid. A similar problem is solved in [41] using a more sophisticated control strategy which requires knowledge of the network dynamics. As in [40, 41], we assume that the phase δ_i and the (angular) frequency ω_i of each generator i obey the swing equation dynamics with the parameters given in [40] (except for generator 1 whose phase and frequency are fixed to a constant, cf. Methods). Initially, each generator operates at a locally stable steady-state condition determined by the power flow equations. At time $t = 2\text{s}$, a three-phase fault occurs in the transmission line connecting nodes 16 and 17. After 0.5s the fault is cleared; however the generators have lost synchrony and deviate from their steady-state values (Fig. 4(b)). To recover the normal behavior of the grid, 0.5s after the clearance of the fault, we apply a short, optimal control input to the frequency of the generators to steer the state (phase and frequency) of the generators back to its steady-state value. The input is computed from data via (4) using $N = 4000$ input/state experiments collected by locally perturbing the state of the generators around its normal operation point (see also Methods). We consider data sampled with period $T_s = 2.5 \times 10^{-4}\text{s}$, and set the control horizon to $T = 400$ time samples (corresponding to 0.1s), $R = I$, and $Q = \varepsilon I$ with $\varepsilon = 0.01$ to enforce locality of the controlled trajectories. As shown in Fig. 4(c), the data-driven input drives the state of the generators to a point close enough to the starting synchronous solution (*left, inset*) so as to asymptotically recover the correct operation of the grid (*right*). Notably, as previously discussed, the computation of the control input requires only pre-collected data, is numerically efficient, and optimal (for the linearized dynamics). More generally, this numerical study suggests that the data-driven strategy (4) could represent a simple, viable, and computationally-efficient approach to control complex non-linear networks around an operating point.

2. Controlling functional brain networks via fMRI snapshots

We investigate the problem of generating prescribed patterns of activity in functional brain networks directly from task-based functional magnetic resonance imaging (task-fMRI) time series. Specifically, we examine a dataset of task-based fMRI experiments related to motor activity extracted from the Human Connectome Project (HCP) [43] (see Fig. 5(a)). In these experiments, participants are presented with visual cues that ask them to execute specific motor tasks; namely, tap their left or right fingers, squeeze their left or right toes, and move their tongue. We consider a set of $m = 6$ input channels associated with different task-related stimuli; that is, the motor tasks' stimuli and the visual cue preceding them. As in [44], we encode the input signals as binary time series taking the value of 1 when the corresponding task-related stimulus occurs and 0 otherwise. The output signals consist of minimally pre-processed blood-oxygen-level-dependent (BOLD) time series associated with the fMRI measurements at different regions of the brain (see also Methods). In our numerical study, we parcellated the brain into $p = 148$ brain regions (74 regions per hemisphere) according to the Destrieux 2009 atlas [45]. Further, as a baseline for comparison, we approximate the dynamics of the functional network with a low-dimensional ($n = 20$) linear model computed via the approach described in [44], which has been shown to accurately capture the underlying network dynamics.

In Fig. 5(b), we plot the inputs (*top*) and outputs (*center*) of one subject for the first sequence of five motor tasks. The bottom plot of the same figure shows the outputs obtained by approximating the network dynamics with the above-mentioned linear model. In Fig. 5(c), we compare the performance of the minimum-energy data-driven control in (5) with the model-based one, assuming that the network obeys the dynamics of the approximate linear model. We choose a control horizon $T = 100$, form the data matrices in (3) by sliding a window of fixed size T over the available fMRI data, and consider a set of 20 orthogonal targets $\{y_{f,i}\}_{i=1}^{20}$ corresponding to eigenvectors of the estimated T -step controllability Gramian (see Methods for further details). The top plot of Fig. 5(c) reports the error (normalized by the output dimension) in the final state of the two strategies, while the bottom plot shows the corresponding control energy (that is, the norm of the control input). In the plots, the targets are ordered from the most ($y_{f,1}$) to the least ($y_{f,20}$) controllable. The data-driven and the model-based inputs exhibit an almost identical behavior with ref-

erence to the most controllable targets. As we shift towards the least controllable targets, the data-driven strategy yields larger errors but, at the same time, requires less energy to be implemented, thus being potentially more feasible in practice. Importantly, since the underlying brain dynamics are not known, errors in the final state are computed using the identified linear dynamical model. It is thus expected that data-driven inputs yield larger errors in the final state than model-based inputs, although these errors may not correspond to control inaccuracies when applying the data-driven inputs to the actual brain dynamics. Ultimately, our numerical study suggests that the data-driven framework could represent a viable alternative to the classic model-based approach (e.g., see [12, 46, 47]) to infer controllability properties of brain networks, and (by suitably modulating the reconstructed inputs) enforce desired functional configurations in a non-invasive manner and without requiring real-time measurements.

III. DISCUSSION

In this paper we present a framework to control complex dynamical networks from data generated by non-optimal (and possibly random) experiments. We show that optimal point-to-point controls to reach a desired target state, including the widely used minimum-energy control input, can be determined exactly from data. We provide closed-form and approximate data-based expressions of these control inputs and characterize the minimum number of samples needed to compute them. Further, we show by means of numerical simulations that data-driven inputs are more accurate and computationally more efficient than model-based ones, and can be used to analyze and manipulate the controllability properties of real networks.

More generally, our framework and results suggest that many network control problems may be solved by simply relying on experimental data, thus promoting a new, exciting, and practical line of research in the field of complex networks. Because of the abundance of data in modern applications and the computationally appealing properties of data-driven controls, we expect that this new line of research will benefit a broad range of research communities, spanning from engineering to biology, which employ control-theoretic methods and tools to comprehend and manipulate complex networked phenomena.

Some limitations of this study should also be acknowledged and discussed. First, in our

work we consider networks governed by linear dynamics. On the one hand, this is a restrictive assumption since many real-world networks are inherently nonlinear. On the other hand, linear models are used successfully to approximate the behavior of nonlinear dynamical networks around desired operating points, and capture more explicitly the impact of the network topology. Second, in many cases a closed-loop control strategy is preferable than a point-to-point one, especially if the control objective is to stabilize an equilibrium when external disturbances corrupt the dynamics. However, we stress that point-to-point controls, in addition to being able to steer the network to arbitrary configurations, are extensively used to characterize the fundamental control properties and limitations in networks of dynamical nodes. For instance, the expressions we provide for point-to-point control can also lead to novel methods to study the energetic limitations of controlling complex networks [9], select sensors and actuators for optimized estimation and control [48], and design optimized network structures [49]. Finally, although we provide data-driven expressions that compensate for the effect of noise in the limit of infinite data, we do not provide non-asymptotic guarantees on the reconstruction error. Overcoming these limitations represents a compelling direction of future work, which can strengthen the relevance and applicability of our data-driven control framework, and ultimately lead to viable control methods for complex networks.

IV. METHODS

A. Model-based expressions of optimal controls

The model-based solution to (2) can be written in batch form as

$$u_{0:T-1}^* = (I - K_{C_T}(MK_{C_T})^\dagger M)\mathcal{C}_T^\dagger y_f, \quad (10)$$

where $\mathcal{C}_T = [CB \ CAB \ \dots \ CA^{T-1}B]$ is the T -step output controllability matrix of the dynamical network in (1), K_{Y_T} denotes a basis of the kernel of \mathcal{C}_T , and M is any matrix

satisfying $M^\top M = \mathcal{H}_T^\top Q \mathcal{H}_T + R$, with

$$\mathcal{H}_T = \begin{bmatrix} 0 & \cdots & \cdots & 0 & CB \\ \vdots & \cdots & 0 & CB & CAB \\ \vdots & \ddots & \ddots & \ddots & \vdots \\ 0 & CB & CAB & \cdots & CA^{T-2}B \end{bmatrix},$$

and 0 entries denoting $p \times m$ zero matrices. If $Q = 0$ and $R = I$ (minimum-energy control input), (10) simplifies to $u_{0:T-1}^* = \mathcal{C}_T^\dagger y_f$. Alternatively, if the network is target controllable, the minimum-energy input can be compactly written as

$$u^*(t) = B^\top A^{T-t-1} C^\top \mathcal{W}_T^{-1} y_f, \quad t = 0, 1, 2, \dots, T-1. \quad (11)$$

where \mathcal{W}_T denotes the T -step output controllability Gramian of the dynamical network in (1)

$$\mathcal{W}_T = \mathcal{C}_T \mathcal{C}_T^\top = \sum_{t=0}^{T-1} CA^t BB^\top (A^\top)^t C^\top, \quad (12)$$

which is invertible if and only if the network is target controllable. Equation (11) is the classic (Gramian-based) expression of the minimum-energy control input [36]. It is well-known that this expression is numerically unstable, even for moderate size systems, e.g., see [20].

B. Subspace-based system identification

Given the data matrices $U_{0:T-1}$ and Y_T as defined in (3) and assuming that $C = I$, a simple deterministic subspace-based procedure [50, Ch. 6] to estimate the matrices A and B from the available data consists of the following two steps:

1. Compute an estimate of the T -step controllability matrix of the network as the solution of the minimization problem

$$\hat{\mathcal{C}}_T = \arg \min_{\mathcal{C}_T} \|Y_T - \mathcal{C}_T U_{0:T-1}\|_F^2, \quad (13)$$

where $\|\cdot\|_F$ denotes the Frobenius norm of a matrix. The solution to (13) has the form $\hat{\mathcal{C}}_T = Y_T U_{0:T-1}^\dagger$.

2. In view of the definition of the controllability matrix, obtain an estimate of the matrix B by extracting the first m columns of $\hat{\mathcal{C}}_T$. Namely, $\hat{B} = [\hat{\mathcal{C}}_T]_{:,1:m}$, where $[X]_{:,i:j}$

indicates the sub-matrix of X obtained from keeping the entries from the i -th to j -th columns and all of its rows. An estimate of the matrix A can be obtained as the solution to the least-squares problem

$$\hat{A} = \arg \min_A \left\| \left[\hat{\mathcal{C}}_T \right]_{:,m+1:mT} - A \left[\hat{\mathcal{C}}_T \right]_{:,1:(T-1)m} \right\|_F^2,$$

which yields the matrix $\hat{A} = [\hat{\mathcal{C}}_T]_{:,m+1:mT} [\hat{\mathcal{C}}_T]_{:,1:(T-1)m}^\dagger$.

If the data are noiseless, the system is controllable in $T - 1$ steps, and $U_{0:T-1}$ has full row rank, then this procedure provably returns correct estimates of A and B [50].

C. Power-grid network dynamics, parameters, and data generation

The short-term electromechanical behavior of generators $\{2, \dots, 10\}$ of the New England power-grid network are modeled by the swing equations [51]:

$$\begin{aligned} \dot{\delta}_i &= \omega_i, \\ \frac{H_i}{\pi f_b} \dot{\omega}_i &= -D_i \omega_i + P_{mi} - G_{ii} E_i^2 + \sum_{j=1, j \neq i}^{10} E_i E_j (G_{ij} \cos(\delta_i - \delta_j) + B_{ij} \sin(\delta_i - \delta_j)). \end{aligned} \quad (14)$$

where δ_i is the angular position or phase of the rotor in generator i with respect to generator 1, and where ω_i is the deviation of the rotor speed or frequency in generator i relative to the nominal angular frequency $2\pi f_b$. The generator 1 is assumed to be connected to an infinite bus, and has constant phase and frequency. The parameters H_i and D_i are the inertia constant and damping coefficient, respectively, of generator i . The parameter G_{ii} is the internal conductance of generator i , and $G_{ij} + iB_{ij}$ (where i is the imaginary unit) is the transfer impedance between generators i and j . The parameter P_{mi} denotes the mechanical input power of generator i and E_i denotes the internal voltage of generator i . The values of parameters f_b , H_i , D_i , G_{ij} , B_{ij} , and P_{mi} in the non-faulty and faulty configuration are taken from [40], while the voltages E_i and initial conditions ($\delta_i(0)$, $\omega_i(0) = 0$) are fixed using a power flow computation. In our numerical study, we discretize the dynamics (14) using a forward Euler method with sampling time $T_s = 2.5 \times 10^{-4}$ s. Data are generated by applying a Gaussian i.i.d. perturbation with zero mean and variance 0.01 to each frequency ω_i . The initial condition of each experiment is computed by adding a Gaussian i.i.d. perturbation with zero mean and variance 0.01 to the steady-state values of δ_i and ω_i of the swing dynamics (14).

D. Task-fMRI dataset, pre-processing pipeline, and identification setup

The motor task fMRI data used in our numerical study are extracted from the HCP S1200 release [43, 52]. The details for data acquisition and experiment design can be found in [52]. The BOLD measurements have been pre-processed according to the minimal pipeline described in [53], and, as in [44], filtered with a band-pass filter to attenuate the frequencies outside the 0.06–0.12 Hz band. Further, as common practice, the effect of the physiological signals (cardiac, respiratory, and head motion signals) is removed from the BOLD measurements by means of the regression procedure in [44]. The data matrices in (3) are generated via a sliding window of fixed length $T = 100$ with initial time in the interval $[-90, 10]$. We assume that the inputs and states are zero for times less than or equal to 10, i.e., the instant at which the first task condition is issued. We approximate the input-output dynamics with a linear model with state dimension $n = 20$ computed using input-output data in the interval $[0, 150]$ and the identification procedure detailed in [44]. When the estimated network matrix A has unstable eigenvalues, we stabilize A by dividing it by $\rho(A) + 0.01$, where $\rho(A)$ denotes the spectral radius of A . Other identification parameters are as in [44].

E. Computational details

All numerical simulations have been performed via standard linear-algebra LAPACK routines available as built-in functions in Matlab[®] R2019b, running on a 2.6 GHz Intel Core i5 processor with 8 GB of RAM. In particular, for the computation of pseudoinverses we use the singular value decomposition method (command `pinv` in Matlab[®]) with a threshold of 10^{-8} .

F. Materials and data availability

Data were provided (in part) by the Human Connectome Project, WU-Minn Consortium (Principal Investigators: David Van Essen and Kamil Ugurbil; 1U54MH091657) funded by the 16 NIH Institutes and Centers that support the NIH Blueprint for Neuroscience Research; and by the McDonnell Center for Systems Neuroscience at Washington University. The code and data used in this study are freely available in the public GitHub repository: https://github.com/baggiogi/data_driven_control.

ACKNOWLEDGEMENTS

This work was supported in part by awards AFOSR-FA9550-19-1-0235 and ARO-71603NSYIP, and by MIUR (Italian Minister for Education) under the initiative “Departments of Excellence” (Law 232/2016).

AUTHOR CONTRIBUTIONS

G.B, D.S.B, and F.P. contributed to the conceptual and theoretical aspects of the study, wrote the manuscript and the Supplement. G.B. carried out the numerical studies and prepared the figures.

COMPETING INTERESTS

The authors declare no competing interests.

REFERENCES

- [1] Levine, S., Pastor, P., Krizhevsky, A., Ibarz, J. & Quillen, D. Learning hand-eye coordination for robotic grasping with deep learning and large-scale data collection. *The International Journal of Robotics Research* **37**, 421–436 (2018).
- [2] Marx, V. Biology: The big challenges of big data. *Nature* **498**, 255–260 (2013).
- [3] Sejnowski, T. J., Churchland, P. S. & Movshon, J. A. Putting big data to good use in neuroscience. *Nature neuroscience* **17**, 1440 (2014).
- [4] Einav, L. & Levin, J. Economics in the age of big data. *Science* **346**, 1243089 (2014).
- [5] Turk-Browne, N. B. Functional interactions as big data in the human brain. *Science* **342**, 580–584 (2013).
- [6] Bose, A. Smart transmission grid applications and their supporting infrastructure. *IEEE Transactions on Smart Grid* **1**, 11–19 (2010).
- [7] Lv, Y., Duan, Y., Kang, W., Li, Z. & Wang, F.-Y. Traffic flow prediction with big data: a deep learning approach. *IEEE Transactions on Intelligent Transportation Systems* **16**, 865–873 (2014).

- [8] Liu, Y. Y., Slotine, J. J. & Barabási, A. L. Controllability of complex networks. *Nature* **473**, 167–173 (2011).
- [9] Pasqualetti, F., Zampieri, S. & Bullo, F. Controllability metrics, limitations and algorithms for complex networks. *IEEE Transactions on Control of Network Systems* **1**, 40–52 (2014).
- [10] Bof, N., Baggio, G. & Zampieri, S. On the role of network centrality in the controllability of complex networks. *IEEE Transactions on Control of Network Systems* **4**, 643–653 (2017).
- [11] Yan, G. *et al.* Spectrum of controlling and observing complex networks. *Nature Physics* **11**, 779–786 (2015).
- [12] Gu, S. *et al.* Controllability of structural brain networks. *Nature Communications* **6** (2015).
- [13] Liu, Y.-Y. & Barabási, A.-L. Control principles of complex systems. *Reviews in Modern Physics* **88**, 035006 (2016).
- [14] Lindmark, G. & Altafini, C. Minimum energy control for complex networks. *Scientific Reports* **8**, 3188–3202 (2018).
- [15] Gonçalves, J. & Warnick, S. Necessary and sufficient conditions for dynamical structure reconstruction of lti networks. *IEEE Transactions on Automatic Control* **53**, 1670–1674 (2008).
- [16] Shandilya, S. G. & Timme, M. Inferring network topology from complex dynamics. *New Journal of Physics* **13**, 013004 (2011).
- [17] Angulo, M. T., Moreno, J. A., Lippner, G., Barabási, A.-L. & Liu, Y.-Y. Fundamental limitations of network reconstruction from temporal data. *Journal of the Royal Society Interface* **14**, 20160966 (2017).
- [18] Achlioptas, D., Clauset, A., Kempe, D. & Moore, C. On the bias of traceroute sampling: or, power-law degree distributions in regular graphs. *Journal of the ACM (JACM)* **56**, 1–28 (2009).
- [19] Handcock, M. S. & Gile, K. J. Modeling social networks from sampled data. *The Annals of Applied Statistics* **4**, 5 (2010).
- [20] Sun, J. & Motter, A. E. Controllability transition and nonlocality in network control. *Physical Review Letters* **110**, 208701 (2013).
- [21] Wang, L.-Z., Chen, Y.-Z., Wang, W.-X. & Lai, Y.-C. Physical controllability of complex networks. *Scientific reports* **7**, 40198 (2017).
- [22] Levine, S., Finn, C., Darrell, T. & Abbeel, P. End-to-end training of deep visuomotor policies. *The Journal of Machine Learning Research* **17**, 1334–1373 (2016).

- [23] Silver, D. *et al.* Mastering the game of Go without human knowledge. *Nature* **550**, 354 (2017).
- [24] Gevers, M. Identification for control: From the early achievements to the revival of experiment design. *European Journal of Control* **11**, 1–18 (2005).
- [25] Brunton, S. L. & Kutz, J. N. *Data-driven science and engineering: Machine learning, dynamical systems, and control* (Cambridge University Press, 2019).
- [26] Lewis, F. L., Vrabie, D. & Vamvoudakis, K. G. Reinforcement learning and feedback control: Using natural decision methods to design optimal adaptive controllers. *IEEE Control Systems Magazine* **32**, 76–105 (2012).
- [27] Recht, B. A tour of reinforcement learning: The view from continuous control. *Annual Review of Control, Robotics, and Autonomous Systems* (2018).
- [28] Bristow, D. A., Tharayil, M. & Alleyne, A. G. A survey of iterative learning control. *IEEE control systems magazine* **26**, 96–114 (2006).
- [29] Åström, K. J. & Wittenmark, B. On self tuning regulators. *Automatica* **9**, 185–199 (1973).
- [30] Markovskiy, I. & Rapisarda, P. Data-driven simulation and control. *International Journal of Control* **81**, 1946–1959 (2008).
- [31] Persis, C. D. & Tesi, P. Formulas for data-driven control: Stabilization, optimality and robustness. *IEEE Transactions on Automatic Control* **65**, 909–924 (2020).
- [32] Bertsekas, D. P. & Tsitsiklis, J. N. *Neuro-dynamic programming*, vol. 5 (Athena Scientific Belmont, MA, 1996).
- [33] Åström, K. J. & Hägglund, T. *PID controllers: theory, design, and tuning*, vol. 2 (Instrument society of America Research Triangle Park, NC, 1995).
- [34] Gao, J., Liu, Y.-Y., D’Souza, R. M. & Barabási, A. L. Target control of complex networks. *Nature communications* **5**, 5415 (2014).
- [35] Klickstein, I., Shirin, A. & Sorrentino, F. Energy scaling of targeted optimal control of complex networks. *Nature communications* **8**, 15145 (2017).
- [36] Kailath, T. *Linear Systems* (Prentice-Hall, 1980).
- [37] Dean, S., Mania, H., Matni, N., Recht, B. & Tu, S. On the sample complexity of the linear quadratic regulator. *Foundations of Computational Mathematics* 1–47 (2019).
- [38] Ben-Israel, A. & Greville, T. N. E. *Generalized inverses: theory and applications*, vol. 15 of *CMS Books in Mathematics* (Springer-Verlag New York, 2003), 2nd edn.

- [39] Paré, P. E., Chetty, V. & Warnick, S. On the necessity of full-state measurement for state-space network reconstruction. In *2013 IEEE Global Conference on Signal and Information Processing*, 803–806 (IEEE, 2013).
- [40] Susuki, Y., Mezić, I. & Hikiyama, T. Coherent swing instability of power grids. *Journal of nonlinear science* **21**, 403–439 (2011).
- [41] Cornelius, S. P., Kath, W. L. & Motter, A. E. Realistic control of network dynamics. *Nature Communications* **4** (2013).
- [42] Simpson-Porco, J. W., Dörfler, F. & Bullo, F. Voltage collapse in complex power grids. *Nature Communications* **7**, 1–8 (2016).
- [43] Van Essen, D. C. *et al.* The WU-Minn human connectome project: an overview. *Neuroimage* **80**, 62–79 (2013).
- [44] Becker, C. O., Bassett, D. S. & Preciado, V. M. Large-scale dynamic modeling of task-fMRI signals via subspace system identification. *Journal of neural engineering* **15**, 066016 (2018).
- [45] Destrieux, C., Fischl, B., Dale, A. & Halgren, E. Automatic parcellation of human cortical gyri and sulci using standard anatomical nomenclature. *Neuroimage* **53**, 1–15 (2010).
- [46] Deng, S. & Gu, S. Controllability analysis of functional brain networks. *arXiv preprint arXiv:2003.08278* (2020).
- [47] Menara, T., Baggio, G., Bassett, D. S. & Pasqualetti, F. A framework to control functional connectivity in the human brain. In *IEEE Conf. on Decision and Control*, 4697–4704 (Nice, France, 2019).
- [48] Summers, T. H., Cortesi, F. L. & Lygeros, J. On submodularity and controllability in complex dynamical networks. *IEEE Transactions on Control of Network Systems* **3**, 91–101 (2016).
- [49] Zhao, S. & Pasqualetti, F. Networks with diagonal controllability gramians: Analysis, graphical conditions, and design algorithms. *Automatica* **102**, 10–18 (2019).
- [50] Katayama, T. *Subspace methods for system identification*. Communications and Control Engineering (Springer-Verlag London, 2005).
- [51] Kundur, P. *Power System Stability and Control* (McGraw-Hill, 1994).
- [52] WU-Minn, HCP 1200 subjects data release reference manual. <https://www.humanconnectome.org> (2017). Accessed: 2020-03-15.
- [53] Glasser, M. F. *et al.* The minimal preprocessing pipelines for the human connectome project. *Neuroimage* **80**, 105–124 (2013).

FIGURES

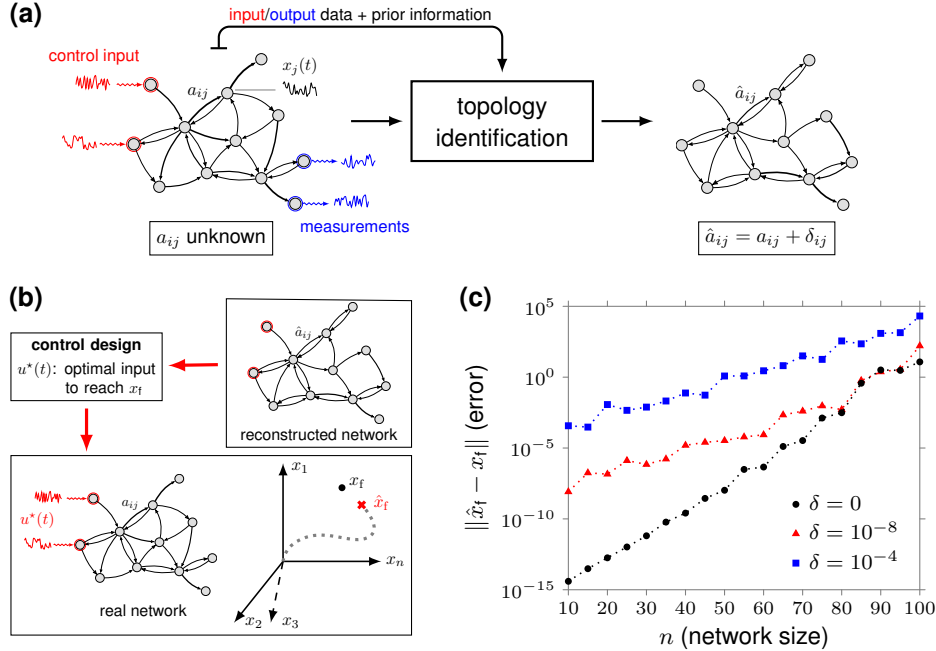


FIG. 1. **The effect of model uncertainty in the computation of optimal network controls.** Panel (a) shows a schematic of a classic network identification procedure. The reconstructed network is affected by estimation errors δ_{ij} . Panel (b) illustrates the error in the final state induced by an optimal control design based on the reconstructed network. In panel (c), we consider minimum-energy controls designed from exact and incorrectly reconstructed networks, and compute the resulting error in the final state as the network size n varies. We consider connected Erdős–Rényi networks with edge probability $p = \ln n/n + 0.1$, 10 randomly selected control nodes, control horizon $T = 2n$, and a randomly chosen final state x_f . Each curve represents the average of the error in the final state over 100 random realizations. To mimic errors in the network reconstruction process, we add to each edge of the network a disturbance modeled as an i.i.d. random variable uniformly distributed in $[-\delta, \delta]$, $\delta > 0$. To compute minimum-energy control inputs, we use the classic Gramian-based formula and standard LAPACK linear algebra routines (see Methods).

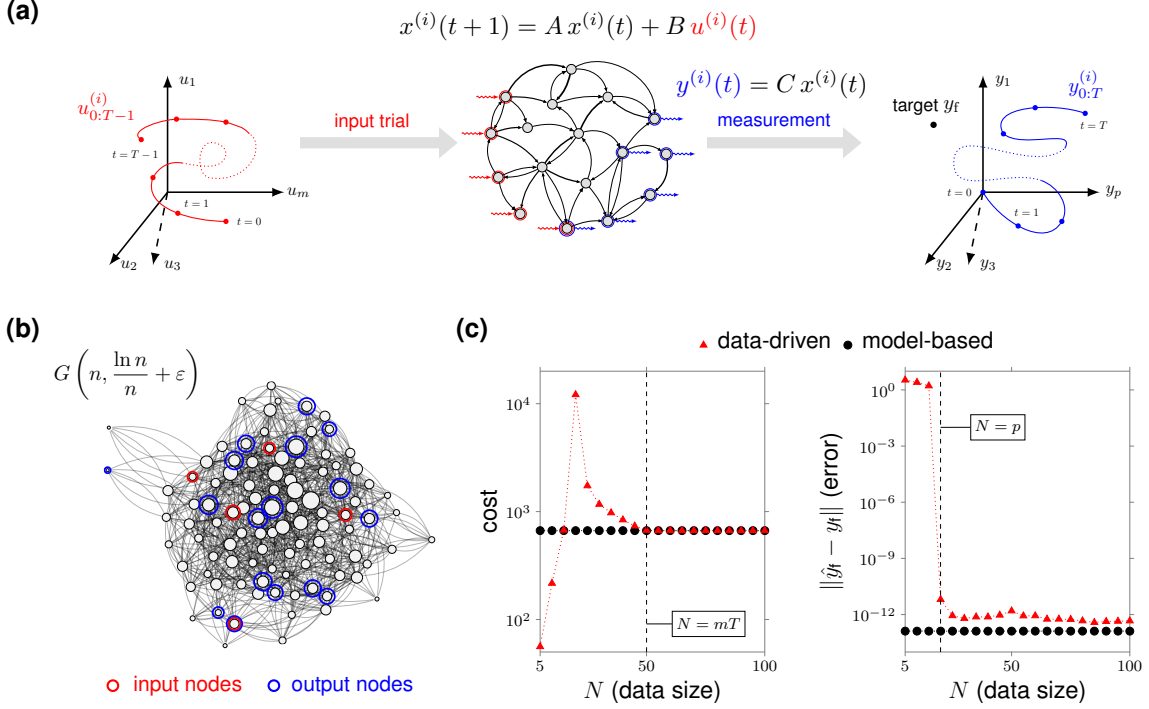


FIG. 2. **Experimental setup and optimal data-driven network controls.** Panel (a) illustrates the data collection process. With reference to the i -th control experiment, a T -step input sequence $u_{0:T}^{(i)}$ excites the network dynamics in (1), and the time samples of the resulting output trajectory $y_{0:T}^{(i)}$ are recorded. The input trajectory $u_{0:T}^{(i)}$ may be generated randomly, so that the final output $y^{(i)}(T)$ does not normally coincide with the desired target output y_f . Red nodes denote the control or input nodes (forming matrix B) and the blue nodes denote the measured or output nodes (forming matrix C). Panel (b) shows a realization of the Erdős–Rényi graph model $G(n, p_{\text{edge}})$ used in our examples, where n is the number of nodes, p_{edge} is the edge probability, m is the number of input nodes (red nodes), and p the number of output nodes (blue nodes). We set the edge probability to $p = \ln n/n + \varepsilon$, $\varepsilon = 0.05$, to ensure connectedness with high probability, and normalize the resulting adjacency matrix by a factor \sqrt{n} . Panel (c) shows the value of the cost function (*left*) and the error in the final state (*right*) for the data-driven input (4) and the model-based control for a randomly chosen target y_f , as a function of the number of data points. We choose $Q = R = I$, $n = 100$, $T = 10$, $m = 5$, and $p = 20$, and consider Erdős–Rényi networks as in panel (b). In all simulations the entries of the input data matrix U are normal i.i.d. random variables, and the input and output nodes are randomly selected. Target controllability is always ensured for all choices of input nodes by adding self-loops and edges that guarantee strong connectivity when needed. All curves represent the average over 500 realizations of data, networks, and input/output nodes. For additional computational details, see Methods.

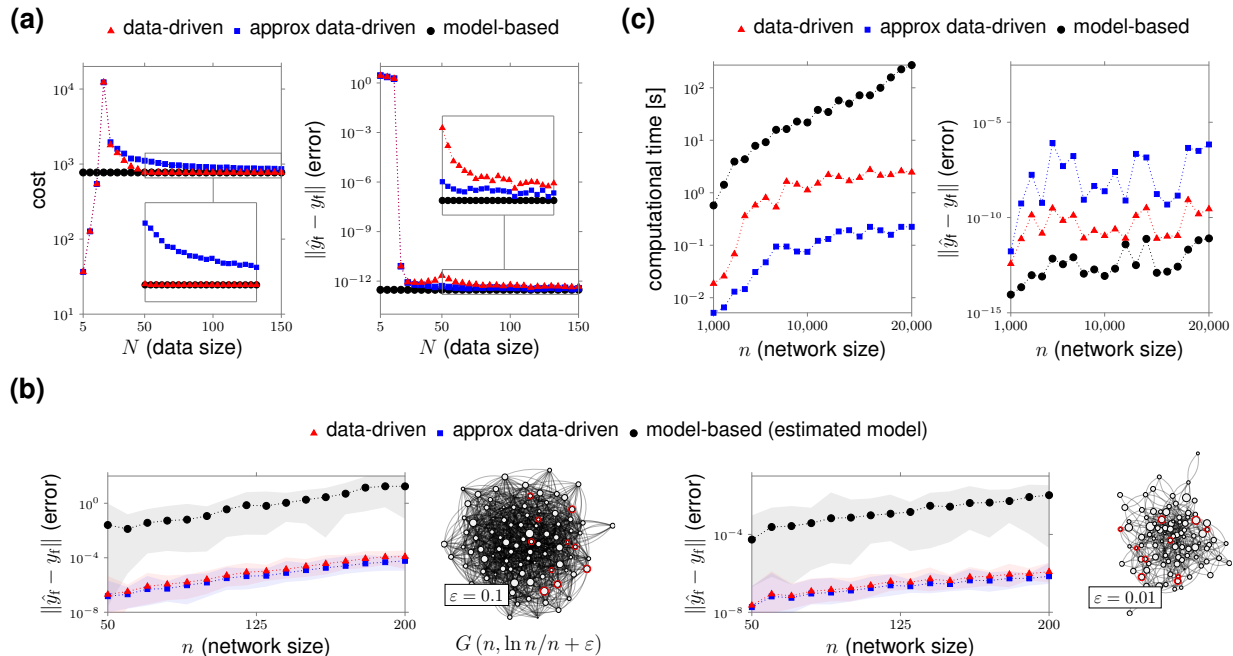


FIG. 3. Performance of minimum-energy data-driven network controls. Panel (a) shows the value of the cost function (*left*) and the error in the final state (*right*) for the minimum-energy data-driven control inputs (5) and (6), and the model-based one as a function of the number of data N . We consider a randomly chosen target y_f , Erdős–Rényi networks as in Fig. 2(b) with $\varepsilon = 0.05$, and parameters $n = 100$, $T = 10$, $m = 5$, $p = 20$. In Panel (b), we compare the error in the final state of the data-driven approach ((5) and (6)), and the classic two-step approach (i.e., network identification followed by model-based control design) for a randomly chosen target y_f , as a function of the network size n . We use the subspace-based identification procedure described in Methods, Erdős–Rényi networks as in Fig. 2(b) with two different edge densities determined through the parameter ε , and parameters $T = 40$, $m = \lfloor n/10 \rfloor$, $p = n$, $N = mT + 10$. The curves in panels (a) and (b) represent the average over 500 realizations of data, networks, and input/output nodes, and the light-colored regions in panel (b) contain the values of all realizations. Panel (c), *left*, compares the time needed to compute the optimal controls via data-driven and model-based strategies as a function of the network size, for a randomly chosen target y_f and one realization of the Erdős–Rényi network model and data. Panel (c), *right*, shows the errors in the final state. We use the following parameters: $\varepsilon = 0.05$, $m = \lfloor n/100 \rfloor$, $p = \lfloor n/50 \rfloor$, $T = 50$, and $N = mT + 100$. In all simulations the entries of the input data matrix $U_{0:T-1}$ are normal i.i.d. variables, and the input and output nodes are randomly selected. Further, target controllability is always ensured for all choices of input nodes by adding self-loops and edges that guarantee strong connectivity when needed. For additional computational details, see Methods.

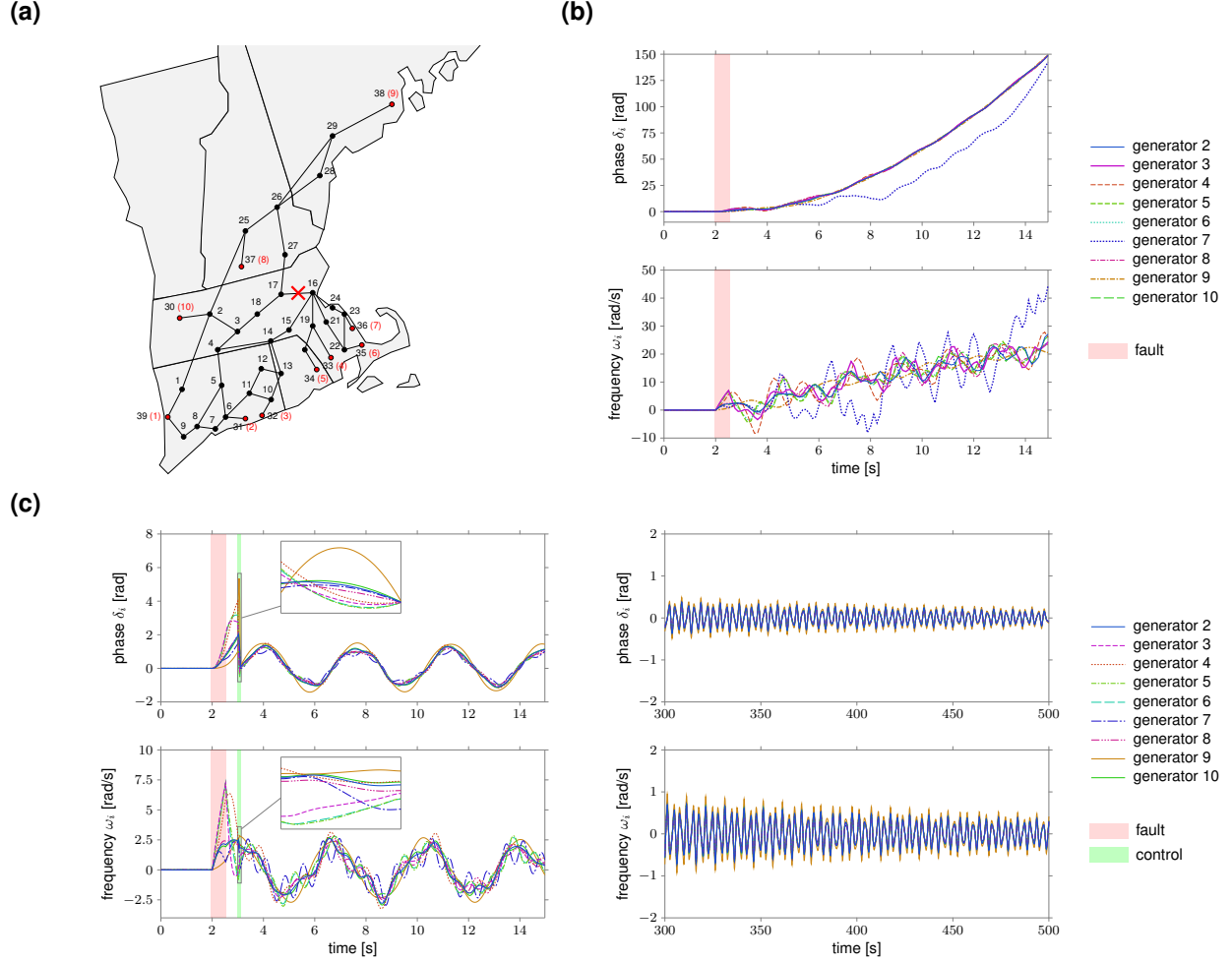


FIG. 4. **Data-driven fault recovery in the New England power-grid network.** Panel (a) depicts the 39-node New England power-grid network. The black nodes $\{1, \dots, 29\}$ represent load nodes, while the red nodes $\{30, \dots, 39\}$ are power generators. The generators are labelled according to the numbers in the red brackets. The red cross denotes the location of the fault. Panel (b) plots the behavior of the phases and frequencies of generators $\{2, \dots, 10\}$ after the occurrence of the fault. The onset time of the fault is $t = 2$ s and the fault duration is 0.5s (red area in the plots). At time $t = 2.5$ s the fault is cleared. The phase and frequency of generator 1 (not shown) are fixed to a constant (see Methods). The left plots of panel (c) show the behavior of the phases and frequencies of generators $\{2, \dots, 10\}$ after the application of the data-driven control input (4). The duration of the control action is 0.1s (green area in the plots) which correspond to a control horizon $T = 400$ for the discretized network dynamics with sampling period $T_s = 2.5 \times 10^{-4}$ s. For the computation of the control input, we employ $N = 4000$ experimental data collected offline by perturbing the state of the generators locally around its steady-state value (see Methods). We use weighting matrices $R = I$ and $Q = \varepsilon I$, where ε is set to a small non-zero constant ($\varepsilon = 0.01$) to guarantee both limited control effort and locality of the controlled trajectories. The insets illustrate the behavior of the phases and frequencies during the application of the control. The right plots of panel (c) show the asymptotic behavior of the phases and frequencies of generators $\{2, \dots, 10\}$ after the application of the data-driven control (4).

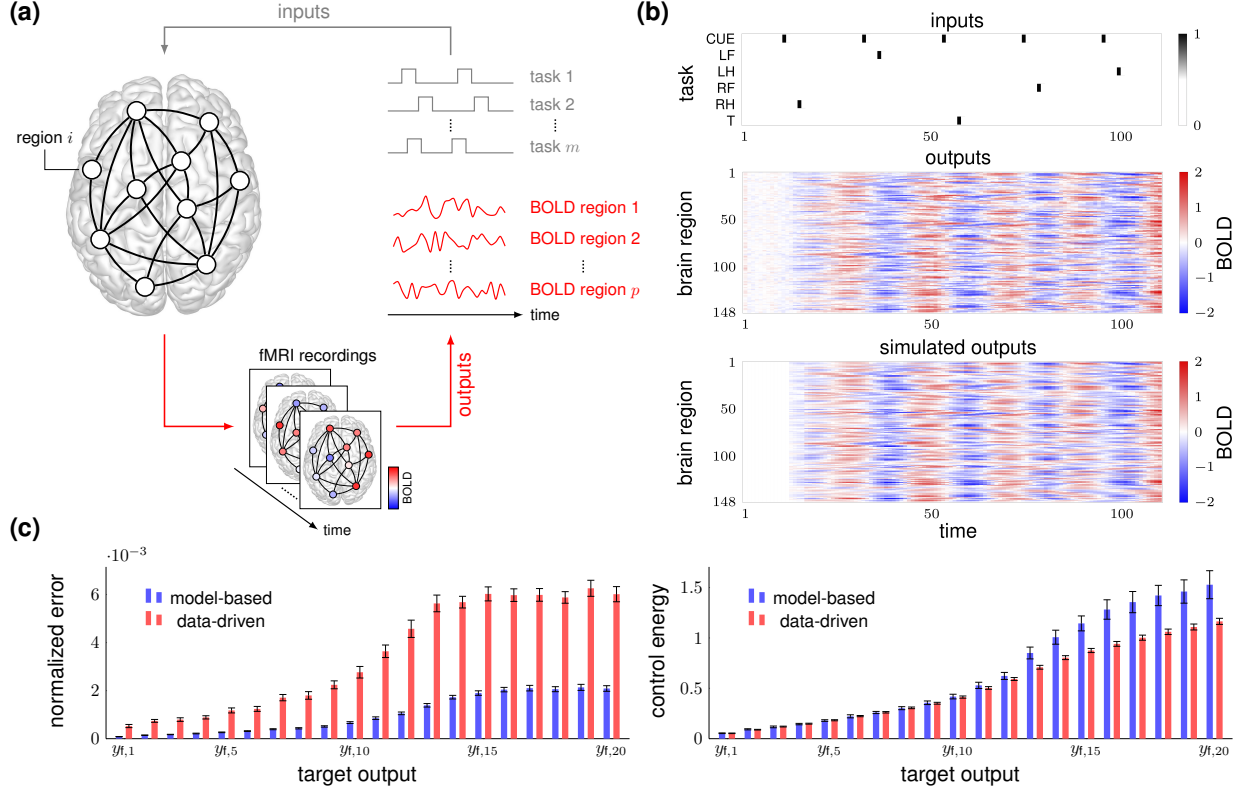


FIG. 5. **Data-driven control of functional brain networks.** Panel (a) provides a schematic of the experimental setup. A set of external stimuli represented by m different task commands induce brain activity. Functional magnetic resonance (fMRI) blood oxygen level dependent (BOLD) signals are measured and recorded at different times and converted into p time series, one for each brain region. The top and center heatmaps of panel (b) show the inputs and outputs, respectively, for the first 110 measurements of one subject of the HCP dataset. The inputs are divided into $m = 6$ channels corresponding to different task conditions, i.e., CUE (a visual cue preceding the occurrence of other task conditions), LF (squeeze left toe), LH (tap left fingers), RF (squeeze right toe), RH (tap right finger), and T (move tongue). As in [44], each input is a binary 0-1 signal taking the value 1 when the corresponding task condition is issued and 0 otherwise. The outputs represent the BOLD signals of the $p = 148$ brain regions obtained from and enumerated according to the Destrieux 2009 atlas [45]. These outputs have been minimally pre-processed following standard techniques [53] as detailed in Methods. The bottom heatmap of panel (b) displays the simulated outputs obtained by exciting the approximate low-dimensional linear model of [44] with the input sequence of the top plot. In panel (c), we compare the performance of the data-driven and model-based strategy, assuming that the dynamics obey the above-mentioned approximate linear model. We set the control horizon to $T = 100$ and generate the data matrices by sliding a time window of size T across the data samples. The target state $y_{f,i}$ is the eigenvector associated with the i -th eigenvalue of the empirical Gramian matrix $\hat{\mathcal{W}}_T = \hat{\mathcal{C}}_T^T \hat{\mathcal{C}}_T$, where $\hat{\mathcal{C}}_T = Y_T U_{0:T-1}^\dagger$. The top plot shows the error to reach the targets $\{y_{f,i}\}_{i=1}^{20}$ using the data-driven minimum-energy input in (5) and the model-based one. The bottom plot shows the norm of the two inputs. The colored bars denote the mean over 100 unrelated subjects and the error bars represent the 95% confidence intervals around the mean.

Supplement to “Data-Driven Control of Complex Networks”

Giacomo Baggio

*Department of Information Engineering,
University of Padova, Padova, Italy*

Danielle S. Bassett

*Departments of Bioengineering, Physics & Astronomy,
Electrical & Systems Engineering, Neurology, and Psychiatry,
University of Pennsylvania, Philadelphia, USA
Santa Fe Institute, Santa Fe, USA*

Fabio Pasqualetti

*Department of Mechanical Engineering,
University of California at Riverside, Riverside, USA*

To whom correspondence should be addressed: fabiopas@engr.ucr.edu

(Dated: August 6, 2020)

CONTENTS

I. Expression of optimal data-driven controls for arbitrary $Q \succeq 0$ and $R \succ 0$	3
II. Minimum number of data to reconstruct $u_{0:T-1}^*$	3
III. Extension to general experimental settings	4
IV. Closed-form expression for $Q = 0$ and $R = I$ (minimum-energy control input)	5
V. Approximate data-driven minimum-energy controls	6
VI. Data-driven optimal control inputs with noisy data	9
A. Data corrupted by small noise	9
B. Data corrupted by i.i.d. noise with zero mean and known variance	9
Supplementary References	13

I. EXPRESSION OF OPTIMAL DATA-DRIVEN CONTROLS FOR ARBITRARY $Q \succeq 0$ AND $R \succ 0$

Consider the data matrices $U_{0:T-1}$, $Y_{1:T-1}$, Y_T as defined in Eq. (3) of the main text. By linearity of the system, a linear combination of the input experiments (columns of $U_{0:T-1}$) yields an output that is a linear combination (with the same coefficients) of the corresponding output data; that is, for any vector $\alpha \in \mathbb{R}^N$, the input $u_{0:T} = U_{0:T}\alpha$ generates the outputs $y_{1:t-1} = Y_{1:T-1}\alpha$ and $y_T = Y_T\alpha$. Assume that there exists a vector α^* such that

$$u_{0:T-1}^* = U_{0:T-1}\alpha^* \quad (1)$$

is the optimal (w.r.t. the cost function in Eq. (2) of the main text) control reaching y_f in T steps. Then, α^* satisfies

$$\begin{aligned} \alpha^* = \arg \min_{\alpha} \quad & \|L\alpha\|_2^2 \\ \text{s.t.} \quad & y_f = Y_T\alpha. \end{aligned} \quad (2)$$

where L is any matrix satisfying $L^\top L = Y_{1:T-1}^\top Q Y_{1:T-1} + U_{0:T-1}^\top R U_{0:T-1}$ ¹ and $\|\cdot\|_2^2$ denotes the ℓ^2 -norm of a vector. From the constraint $y_f = Y_T\alpha$, the optimal α^* has the form $\alpha^* = Y_T^\dagger y_f + K_{Y_T} w^*$, with w^* being any vector such that

$$w^* = \arg \min_w \quad \left\| L(Y_T^\dagger y_f + K_{Y_T} w) \right\|_2^2, \quad (3)$$

where K_{Y_T} denotes a matrix whose columns form a basis of the kernel of Y_T . The solutions to the latter problem are of the form $w^* = -(LK_{Y_T})^\dagger LY_T^\dagger y_f + K_{LY_T} v$, where K_{LY_T} is a matrix whose columns form a basis of $\text{Ker}(LY_T)$ and v is an arbitrary vector. Since $\text{Ker}(LY_T) \subseteq \text{Ker}(Y_T)$, the optimal vector α^* is unique and of the form $\alpha^* = (I - K_{Y_T}(LK_{Y_T})^\dagger L)Y_T^\dagger y_f$. This implies that the (unique) optimal control $u_{0:T-1}^*$ to reach y_f in T steps (that is, (1)) can be written as

$$u_{0:T-1}^* = U_{0:T-1}\alpha^* = U_{0:T-1}(I - K_{Y_T}(LK_{Y_T})^\dagger L)Y_T^\dagger y_f. \quad (4)$$

II. MINIMUM NUMBER OF DATA TO RECONSTRUCT $u_{0:T-1}^*$

If the columns of $U_{0:T-1}$ span the space of all possible input sequences \mathbb{R}^{mT} , that is $U_{0:T-1}$ is full-row rank, then there always exists a vector α^* satisfying $u_{0:T-1}^* = U_{0:T-1}\alpha^*$, for any y_f .

¹ Notice that such a matrix L always exists since $Q \succeq 0$ and $R \succ 0$ imply that $Y_{1:T-1}^\top Q Y_{1:T-1} + U_{0:T-1}^\top R U_{0:T-1} \succeq 0$.

Hence, mT linearly independent data are sufficient to reconstruct the optimal control via (4). In contrast, since any linear combination of optimal control inputs is still an optimal control input (for an output y_f which is the linear combination of the ones reached by the available optimal inputs), if $U_{0:T-1}$ contains p linearly independent and optimal data, then (4) yields the optimal control input, for any target y_f . Thus, at least p linearly independent data must be collected to reconstruct the optimal control input via (4). Finally, we observe that if p linearly independent (and possibly non-optimal) data are available, then Y_T has full row rank and the optimal vector α^* in (2) satisfies the constraint $y_f = Y_T \alpha^*$, so that the resulting control in (4), although in general suboptimal, still correctly steers the output to the desired target y_f , for any choice of y_f .

III. EXTENSION TO GENERAL EXPERIMENTAL SETTINGS

When the initial state of the network is different from $x(0) = 0$ across the experiments, then the optimal control input can be still reconstructed from data, provided that the initial state of each experiment can be measured. In this case, data may consist of a single uninterrupted input/output trajectory of the system, where different control experiments correspond to different segments of length T of this trajectory.

Let $X_0 = \begin{bmatrix} x_0^{(1)} & x_0^{(2)} & \dots & x_0^{(N)} \end{bmatrix} \in \mathbb{R}^{n \times N}$ denote the matrix whose columns consist of the initial states of all control experiments, and K_{X_0} denote a basis of $\text{Ker}(X_0)$. Note that an input sequence $u_{0:T-1}$ expressed as a linear combination of the columns of $U_{0:T-1} K_{X_0}$ yields an output trajectory $y_{1:T}$ which is a linear combination (with the same coefficients) of the columns of $Y_{1:T} K_{X_0}$. Indeed, for any $\alpha \in \mathbb{R}^d$, $d = \dim \text{Ker}(X_0)$, by linearity of the system, we can rewrite the output data Y_T as a sum of a term depending only on X_0 (free response) and a term depending only on $U_{0:T-1}$ (forced response), so that

$$Y_{1:T} K_{X_0} \alpha = (G X_0 + H U_{0:T-1}) K_{X_0} \alpha = H U_{0:T-1} K_{X_0} \alpha, \quad (5)$$

where G , H are matrices of appropriate dimensions that depend on network matrices A , B , C . Thus, assuming that there exists a vector α^* such that $u_{0:T-1}^* = U_{0:T-1} K_{X_0} \alpha^*$ is the optimal control reaching y_f in T steps, it holds that

$$\begin{aligned} \alpha^* = \arg \min_{\alpha} \quad & \|L K_{X_0} \alpha\|_2^2 \\ \text{s.t.} \quad & y_f = Y_T K_{X_0} \alpha. \end{aligned} \quad (6)$$

Hence, along the same lines as before, the optimal control input $u_{0:T-1}^*$ to reach y_f in T steps is given by

$$u_{0:T-1}^* = U_{0:T-1}K_{X_0}(I - K_{Y_T K_{X_0}}(LK_{Y_T K_{X_0}})^\dagger L)(Y_T K_{X_0})^\dagger y_f, \quad (7)$$

where $K_{Y_T K_{X_0}}$ is a matrix whose columns form a basis of $\text{Ker}(Y_T K_{X_0})$. Notice that, if $U_{0:T-1}K_{X_0}$ is full row rank, then there always exists a vector α^* such that $u_{0:T-1}^* = U_{0:T-1}K_{X_0}\alpha^*$, for any target y_f . A sufficient (yet not necessary) condition for $U_{0:T-1}K_{X_0}$ to be full row rank is that $[U_{0:T-1}^\top X_0^\top]^\top$ is full row rank.² This in turn implies that (at most) $mT + n$ linearly independent experiments (w.r.t. to inputs and initial states) suffice to reconstruct the optimal control via (7).

IV. CLOSED-FORM EXPRESSION FOR $Q = 0$ AND $R = I$ (MINIMUM-ENERGY CONTROL INPUT)

For $Q = 0$ and $R = I$, we have that $L = I$ and the data-driven expression in (4) becomes

$$u_{0:T-1}^* = (I - U_{0:T-1}K_{Y_T}(U_{0:T-1}K_{Y_T})^\dagger)U_{0:T-1}Y_T^\dagger y_f. \quad (8)$$

(8) equals the minimum-energy control input to reach y_f in T steps [1], if mT linearly independent input experiments are collected. (8) can be further simplified by exploiting the following instrumental result.

Lemma IV.1. *Let $A \in \mathbb{R}^{r \times n}$, $B \in \mathbb{R}^{q \times n}$. If $\text{Ker}(A) \subseteq \text{Ker}(B)$, then $(I - AK_B(AK_B)^\dagger)AB^\dagger = (BA^\dagger)^\dagger$, where K_B is a matrix whose columns are a basis of $\text{Ker}(B)$.*

Proof. We show that $(I - AK_B(AK_B)^\dagger)AB^\dagger$ satisfies the four conditions [2] defining the Moore–Penrose pseudoinverse of BA^\dagger . To this aim, let $\Pi := I - AK_B(AK_B)^\dagger$. By noticing that $\Pi = \Pi^\top$ is the orthogonal projection onto $\text{Ker}((AK_B)^\top)$, we have

$$(AK_B)^\top \Pi = 0 \implies \Pi AK_B = 0 \implies \Pi AB^\dagger B = \Pi A. \quad (9)$$

By assumption $\text{Ker}(A) \subseteq \text{Ker}(B)$, which implies

$$B(I - A^\dagger A) = 0 \implies BA^\dagger A = B, \quad (10)$$

² Indeed, if $[U_{0:T-1}^\top X_0^\top]^\top$ is full row rank, for all $u \in \mathbb{R}^{mT}$ there exists $\gamma \in \text{Ker}(X_0)$ such that $[u^\top 0^\top]^\top = [U_{0:T-1}^\top X_0^\top]^\top \gamma$, which implies that $U_{0:T-1}K_{X_0}$ must be of full row rank.

since $I - A^\dagger A$ is the orthogonal projection onto $\text{Ker}(A)$. Further, since $BK_B = 0$, we have

$$BA^\dagger(I - \Pi) = BA^\dagger AK_B(AK_B)^\dagger \stackrel{(10)}{=} BK_B(AK_B)^\dagger = 0. \quad (11)$$

Finally, since $I - AA^\dagger$ equals the orthogonal projection onto $\text{Ker}(A^\top)$, and $I - \Pi = AK_B(AK_B)^\dagger$ equals the orthogonal projection onto $\text{Im}(AK_B) \subseteq \text{Im}(A) \perp \text{Ker}(A^\top)$, where $\text{Im}(\cdot)$ denotes the image or column space of a matrix, we have

$$(I - \Pi)(I - AA^\dagger) = [(I - \Pi)(I - AA^\dagger)]^\top = 0 \implies AA^\dagger \Pi = \Pi AA^\dagger, \quad (12)$$

where the last implication follows because $I - \Pi$ and $I - AA^\dagger$ are symmetric. To conclude, we show that $\Pi AB^\dagger = (BA^\dagger)^\dagger$ by proving the four Moore–Penrose conditions [2]:

1. $\Pi AB^\dagger BA^\dagger \Pi AB^\dagger \stackrel{(9)}{=} \Pi AA^\dagger \Pi AB^\dagger \stackrel{(12)}{=} \Pi^2 AA^\dagger AB^\dagger = \Pi AB^\dagger$;
2. $BA^\dagger \Pi AB^\dagger BA^\dagger \stackrel{(9)}{=} BA^\dagger \Pi AA^\dagger = BA^\dagger AA^\dagger - BA^\dagger(I - \Pi)AA^\dagger \stackrel{(11)}{=} BA^\dagger$;
3. $BA^\dagger \Pi AB^\dagger = BA^\dagger AB^\dagger - BA^\dagger(I - \Pi)AB^\dagger \stackrel{(10),(11)}{=} BB^\dagger = (BB^\dagger)^\top$;
4. $\Pi AB^\dagger BA^\dagger \stackrel{(9)}{=} \Pi AA^\dagger \stackrel{(12)}{=} AA^\dagger \Pi = (\Pi AA^\dagger)^\top$.

This concludes the proof. □

Since $Y_T = \mathcal{C}_T U_{0:T-1}$, where $\mathcal{C}_T = [CB \ CAB \ \dots \ CA^{T-1}B]$ is the T -steps output controllability matrix of the network, it holds that $\text{Ker}(U_{0:T-1}) \subseteq \text{Ker}(Y_T)$. Thus, by Lemma IV.1, (7) can be compactly rewritten as

$$u_{0:T-1}^* = (Y_T U_{0:T-1}^\dagger)^\dagger y_t. \quad (13)$$

When the optimal input can be reconstructed from the available data, (13) could also be derived by “direct” estimation of the output controllability matrix \mathcal{C}_T . However, we remark that, based on Lemma IV.1, the data-driven expressions in (7) and (13) are equivalent even when the optimal input cannot be reconstructed from the available data.

V. APPROXIMATE DATA-DRIVEN MINIMUM-ENERGY CONTROLS

Consider the data-driven control input

$$\hat{u}_{0:T-1} = U_{0:T-1} Y_T^\dagger y_t. \quad (14)$$

Notice that $\hat{u}_{0:T-1}$ correctly steers the network to y_f in T steps, as long as p linearly independent experiments are available. Indeed, if Y_T is full row rank, there exists $\bar{\alpha} \in \mathbb{R}^N$ satisfying $y_f = Y_T \bar{\alpha}$, for all y_f , so that $\hat{u}_{0:T-1} = U_{0:T-1} \bar{\alpha} = U_{0:T-1} Y_T^\dagger y_f$ drives the network to y_f . Although $\hat{u}_{0:T-1}$ does not typically coincide with the minimum-energy control, when the input experiments are generated randomly and independently from a Gaussian distribution, $\hat{u}_{0:T-1}$ approaches the minimum-energy control as the number of experiments grows, as we show next. To this end we need the following standard result in non-asymptotic random matrix theory, e.g., see [3, Corollary 5.35 and Lemma 5.36]. Given a matrix $X \in \mathbb{R}^{n \times m}$, $\sigma_{\min}(A)$, $\sigma_{\max}(A)$, and $\kappa(A) := \sigma_{\max}(A)/\sigma_{\min}(A)$ denote the largest, smallest (non-zero) singular value, and the condition number of A , respectively.

Lemma V.1. *Let $X \in \mathbb{R}^{N \times q}$ have i.i.d. normally distributed entries. Then, with probability at least $1 - \delta$*

$$\left\| \frac{1}{N} X^\top X - I \right\|_2 \leq 3 \max(\eta, \eta^2),$$

$$1 - \eta \leq \sigma_{\min} \left(\frac{1}{\sqrt{N}} X \right) \leq \sigma_{\max} \left(\frac{1}{\sqrt{N}} X \right) \leq 1 + \eta,$$

where $\eta := \sqrt{q/N} + \sqrt{2 \ln(1/\delta)/N}$ and $\|X\|_2 = \sigma_{\max}(X)$ denotes the spectral norm of matrix X .

Theorem V.2. *Assume that the network is output controllable, $U_{0:T-1}$ has full row rank, and the entries of $U_{0:T-1}$ are i.i.d. Gaussian random variables with zero mean and finite variance $\sigma^2 \neq 0$. Then, with probability at least $1 - \delta$*

$$\|u_{0:T-1}^* - \hat{u}_{0:T-1}\|_2 \leq \frac{3 \max(\eta, \eta^2)}{\sigma_{\min}(\mathcal{C}_T)} \left(1 + \frac{1 + \eta}{1 - \eta} \kappa^2(\mathcal{C}_T) \right) \|y_f\|_2, \quad (15)$$

where $u_{0:T-1}^*$ is the minimum-energy control input driving the network to y_f , the matrix $\mathcal{C}_T = [CB \ CAB \ \dots \ CA^{T-1}B]$ is the T -steps output controllability matrix of the network, and $\eta := \sqrt{mT/N} + \sqrt{2 \ln(1/\delta)/N}$. In particular, as $N \rightarrow \infty$,

$$\hat{u}_{0:T-1} \xrightarrow{a.s.} u_{0:T-1}^*, \quad (16)$$

where $\xrightarrow{a.s.}$ stands for almost sure convergence.

Proof. Since $Y_T = \mathcal{C}_T U_{0:T-1}$, the data-driven input in (14) can be written as

$$\hat{u}_{0:T-1} = U_{0:T-1} (\mathcal{C}_T U_{0:T-1})^\dagger y_f = \frac{1}{\sigma^2 N} U_{0:T-1} U_{0:T-1}^\top \mathcal{C}_T^\top \left(\frac{1}{\sigma^2 N} \mathcal{C}_T U_{0:T-1} U_{0:T-1}^\top \mathcal{C}_T^\top \right)^{-1} y_f, \quad (17)$$

where we used that $X^\dagger = X^\top(XX^\top)^{-1}$, if X has full row rank, e.g., see [2]. By using the above expression and the fact that $u_{0:T-1}^* = \mathcal{C}_T^\dagger y_f$ [1], we have

$$e := u_{0:T-1}^* - \hat{u}_{0:T-1} = \left[\mathcal{C}_T^\dagger - \frac{1}{\sigma^2 N} U_{0:T-1} U_{0:T-1}^\top \mathcal{C}_T^\top \left(\frac{1}{\sigma^2 N} \mathcal{C}_T U_{0:T-1} U_{0:T-1}^\top \mathcal{C}_T^\top \right)^{-1} \right] y_f. \quad (18)$$

By defining the matrix $V_{0:T-1} := U_{0:T-1} U_{0:T-1}^\top - \sigma^2 NI$, the latter equation can be written as

$$\begin{aligned} e &= \left[\mathcal{C}_T^\dagger - \frac{1}{\sigma^2 N} (V_{0:T-1} + \sigma^2 NI) \mathcal{C}_T^\top \left(\frac{1}{\sigma^2 N} \mathcal{C}_T V_{0:T-1} \mathcal{C}_T^\top + \mathcal{C}_T \mathcal{C}_T^\top \right)^{-1} \right] y_f \\ &= \left[\mathcal{C}_T^\dagger - \frac{1}{\sigma^2 N} (V_{0:T-1} + \sigma^2 NI) \mathcal{C}_T^\top \left((\mathcal{C}_T \mathcal{C}_T^\top)^{-1} - \left(\frac{1}{\sigma^2 N} \mathcal{C}_T V_{0:T-1} \mathcal{C}_T^\top + \mathcal{C}_T \mathcal{C}_T^\top \right)^{-1} \right. \right. \\ &\quad \left. \left. \cdot \frac{1}{\sigma^2 N} \mathcal{C}_T V_{0:T-1} \mathcal{C}_T^\top (\mathcal{C}_T \mathcal{C}_T^\top)^{-1} \right) \right] y_f \\ &= \left[-I + \frac{1}{\sigma^2 N} U_{0:T-1} U_{0:T-1}^\top \mathcal{C}_T^\top \left(\frac{1}{\sigma^2 N} \mathcal{C}_T U_{0:T-1} U_{0:T-1}^\top \mathcal{C}_T^\top \right)^{-1} \mathcal{C}_T \right] \frac{1}{\sigma^2 N} V_{0:T-1} \mathcal{C}_T^\dagger y_f, \quad (19) \end{aligned}$$

where in the second step we used the matrix identity $(X + Y)^{-1} = Y^{-1} - (X + Y)^{-1} X Y^{-1}$, which holds for square matrices X, Y with Y and $X + Y$ being non-singular (e.g., see [4, p. 151]), and in the last step the identity $\mathcal{C}_T^\dagger = \mathcal{C}_T^\top (\mathcal{C}_T \mathcal{C}_T^\top)^{-1}$ which follows from the fact that \mathcal{C}_T has full row rank because the network is output controllable by assumption. Thus, from (19), the triangle inequality and the submultiplicativity of the 2-norm:

$$\begin{aligned} \|e\|_2 &\leq \left(1 + \left\| \frac{1}{\sigma^2 N} U_{0:T-1} U_{0:T-1}^\top \mathcal{C}_T^\top \left(\frac{1}{\sigma^2 N} \mathcal{C}_T U_{0:T-1} U_{0:T-1}^\top \mathcal{C}_T^\top \right)^{-1} \mathcal{C}_T \right\|_2 \right) \left\| \frac{1}{\sigma^2 N} V_{0:T-1} \mathcal{C}_T^\dagger y_f \right\|_2 \\ &\leq \left(1 + \left\| \frac{1}{\sigma^2 N} U_{0:T-1} U_{0:T-1}^\top \right\|_2 \left\| \mathcal{C}_T \right\|_2 \left\| \left(\frac{1}{\sigma^2 N} \mathcal{C}_T U_{0:T-1} U_{0:T-1}^\top \mathcal{C}_T^\top \right)^{-1} \right\|_2 \right) \left\| \frac{1}{\sigma^2 N} V_{0:T-1} \right\|_2 \\ &\quad \cdot \left\| \mathcal{C}_T^\dagger \right\|_2 \|y_f\|_2 \\ &\leq \left(1 + \frac{\sigma_{\max} \left(\frac{1}{\sqrt{\sigma^2 N}} U_{0:T-1} \right) \sigma_{\max}^2(\mathcal{C}_T)}{\sigma_{\min} \left(\frac{1}{\sqrt{\sigma^2 N}} U_{0:T-1} \right) \sigma_{\min}^2(\mathcal{C}_T)} \right) \frac{\left\| \frac{1}{\sigma^2 N} V_{0:T-1} \right\|_2}{\sigma_{\min}(\mathcal{C}_T)} \|y_f\|_2, \quad (20) \end{aligned}$$

where in the last step we used that $\sigma_{\min}(XY) \geq \sigma_{\min}(X)\sigma_{\min}(Y)$ ³ and $\|X^\dagger\| = \sigma_{\min}^{-1}(X)$, for matrices X, Y with full row rank. The result now follows from (20), by invoking Lemma V.1. \square

³ Indeed, if X, Y have full row rank, it holds $\sigma_{\min}(XY) = \lambda_{\min}(XY Y^\top X^\top) \geq \lambda_{\min}(Y Y^\top) \lambda_{\min}(X X^\top) = \sigma_{\min}(X)\sigma_{\min}(Y)$, where $\lambda_{\min}(\cdot)$ denotes the smallest eigenvalue of a symmetric matrix and we used that $P \succeq \lambda_{\min}(P)I$ if $P \succeq 0$.

From the non-asymptotic bound in (15) of Theorem VI.1, for a fixed number N of i.i.d. Gaussian data, the larger $\sigma_{\min}(\mathcal{C}_T)$ is, the closer the data-driven input in (14) to the minimum-energy one is. Since $\sigma_{\min}^{-1}(\mathcal{C}_T)$ equals the worst-case control energy required to reach a unit-norm target [5], it follows that networks that are “easy” to control (i.e., networks featuring a large $\sigma_{\min}(\mathcal{C}_T)$) yield the most favorable approximation performance. In other words, the more “excitable” the network dynamics [6] (i.e., the larger $\sigma_{\min}(\mathcal{C}_T)$) are, the lower the approximation error is.

VI. DATA-DRIVEN OPTIMAL CONTROL INPUTS WITH NOISY DATA

A. Data corrupted by small noise

Consider the minimum-energy data-driven expressions (13), (14), and assume that the data matrices $U_{0:T-1}$, Y_T have full (row) rank. Since the Moore–Penrose pseudoinverse of a full (row or column) rank matrix X is a continuous function of the entries of X (in the set of matrices preserving the rank of X) [2, Ch. 6], it follows that (13) and (14) are continuous functions of the data matrices around their true values. Thus, small perturbations of the entries of $U_{0:T-1}$, Y_T , yield a small deviation of the data-driven expressions (13) and (14) from their correct values. A similar argument applies to the optimal data-driven control (4), provided that the singular values of the pseudoinverse of LK_{Y_T} (which is not typically of full rank) are truncated by small constant $\varepsilon > 0$ to preserve the rank of LK_{Y_T} when small perturbations are applied to the data matrices $Y_{1:T-1}$ and Y_T .

B. Data corrupted by i.i.d. noise with zero mean and known variance

We assume that the data matrices $U_{0:T-1}$, $Y_{1:T-1}$, Y_T are corrupted by i.i.d. noise with zero mean and finite variance. Namely, we consider the following dataset

$$\begin{aligned} U_{0:T-1} &= \bar{U}_{0:T-1} + \Delta_U, \\ Y_{1:T-1} &= \bar{Y}_{1:T-1} + \Delta_Y, \\ Y_T &= \bar{Y}_T + \Delta_{Y_T}, \end{aligned} \tag{21}$$

where $\bar{U}_{0:T-1}$, $\bar{Y}_{1:T-1}$, and \bar{Y}_T denote the ground truth values, whereas Δ_U , Δ_Y , and Δ_{Y_T} are independent random matrices with i.i.d. entries with zero mean and variance σ_U^2 , σ_Y^2 , and

$\sigma_{Y_T}^2$, respectively.

The data-driven controls in (4), (8), (13), and (14) computed from the noisy data in (21) are typically biased and do not converge to the true control input as the data size N grows to infinity. For a concrete example of the latter fact, consider the approximate data-driven control in (14), the scalar ($p = m = 1$) system $x(t+1) = Ax(t) + u(t)$, $y(t) = x(t)$, and a unitary control horizon ($T = 1$). In this simple scenario, (14) simplifies to

$$\hat{u}_0 = \frac{\sum_{i=1}^N u_1^{(i)} y_1^{(i)}}{\sum_{i=1}^N (y_1^{(i)})^2} = \frac{\sum_{i=1}^N (\bar{u}_1^{(i)} + \delta_U^{(i)}) (\bar{y}_1^{(i)} + \delta_{Y_T}^{(i)})}{\sum_{i=1}^N (\bar{y}_1^{(i)} + \delta_{Y_T}^{(i)})^2}, \quad (22)$$

where $\bar{U}_0 = [\bar{u}_0^{(1)} \cdots \bar{u}_0^{(1)}]$, $\bar{Y}_1 = [\bar{y}_1^{(1)} \cdots \bar{y}_1^{(N)}]$, and $\Delta_U = [\delta_U^{(1)} \cdots \delta_U^{(N)}]$, $\Delta_{Y_T} = [\delta_{Y_T}^{(1)} \cdots \delta_{Y_T}^{(N)}]$ denote the true data and noise samples, respectively. By the Strong Law of Large Numbers [7] and the assumption on the noise, as $N \rightarrow \infty$, it follows that

$$\hat{u}_0 = \frac{\frac{1}{N} \sum_{i=1}^N (\bar{u}_1^{(i)} + \delta_U^{(i)}) (\bar{y}_1^{(i)} + \delta_{Y_T}^{(i)})}{\frac{1}{N} \sum_{i=1}^N (\bar{y}_1^{(i)} + \delta_{Y_T}^{(i)})^2} \xrightarrow{\text{a.s.}} \frac{\frac{1}{N} \sum_{i=1}^N \bar{u}_1^{(i)} \bar{y}_1^{(i)}}{\frac{1}{N} \sum_{i=1}^N (\bar{y}_1^{(i)})^2 + \sigma_{Y_T}^2}. \quad (23)$$

Because of the variance term $\sigma_{Y_T}^2$ in the denominator, \hat{u}_0 does not converge to the noiseless control input. To remedy this situation, one could modify the data-driven expressions in order to compensate for the variance of the noise, as we detail next.

We first consider the data-driven control in (4) and rewrite it as

$$\begin{aligned} \hat{u}_{0:T-1} &= U_{0:T-1} \left(I - K_{Y_T} (L K_{Y_T})^\dagger L^\top \right) Y_T^\dagger y_f \\ &= U_{0:T-1} \left(I - \Pi_{Y_T} L^\top (L \Pi_{Y_T} L^\top)^\dagger L \right) Y_T^\top (Y_T Y_T^\top)^\dagger y_f, \end{aligned} \quad (24)$$

where $\Pi_{Y_T} = K_{Y_T} K_{Y_T}^\top = I - Y_T^\dagger Y_T = I - Y_T^\top (Y_T Y_T^\top)^\dagger Y_T$ denote the orthogonal projection onto $\text{Ker}(Y_T)$ and we used that $X^\dagger = X^\top (X X^\top)^\dagger$, for any matrix X , e.g., see [2]. Next, we consider the following ‘‘corrected’’ version of (24)

$$\hat{u}_{0:T-1}^{(c)} = U_{0:T-1} \left(I - \tilde{\Pi}_{Y_T} L^\top \left(L \Pi_{Y_T} L^\top - \begin{bmatrix} N\sigma_Y^2 Q & 0 \\ 0 & N\sigma_U^2 R \end{bmatrix} \right)^\dagger L \right) Y_T^\top (Y_T Y_T^\top - N\sigma_{Y_T}^2 I)^\dagger y_f, \quad (25)$$

where $\tilde{\Pi}_{Y_T} = I - Y_T^\top (Y_T Y_T^\top - N\sigma_{Y_T}^2 I)^\dagger Y_T$, L is the particular square root

$$L := \begin{bmatrix} Q^{1/2} Y_{1:T-1} \\ R^{1/2} U_{0:T-1} \end{bmatrix}, \quad (26)$$

and X_ε^\dagger denotes the Moore–Penrose pseudoinverse of X that treats as zero the singular values of X that are smaller than $\varepsilon > 0$.

Theorem VI.1. Consider the noisy dataset as in (21) and assume that $\bar{U}_{0:T-1}$ has full row rank. For $\varepsilon > 0$ sufficiently small and $N \rightarrow \infty$, the control sequence in (25) converges almost surely to the optimal control input; that is,

$$\hat{u}_{0:T-1}^{(c)} \xrightarrow{\text{a.s.}} u_{0:T-1}^*. \quad (27)$$

Proof. After some algebraic manipulations, (25) can be written as

$$\begin{aligned} \hat{u}_{0:T-1}^{(c)} &= U_{0:T-1} \left(I - \tilde{\Pi}_{Y_T} L^\top \left(L \Pi_{Y_T} L^\top - \begin{bmatrix} N\sigma_Y^2 Q & 0 \\ 0 & N\sigma_U^2 R \end{bmatrix} \right)^\dagger_\varepsilon L \right) Y_T^\top (Y_T Y_T^\top - N\sigma_{Y_T}^2 I)^\dagger y_f \\ &= U_{0:T-1} Y_T^\top (Y_T Y_T^\top - N\sigma_{Y_T}^2 I)^\dagger y_f - U_{0:T-1} \tilde{\Pi}_{Y_T} L^\top \cdot \\ &\quad \cdot \left(L \Pi_{Y_T} L^\top - \begin{bmatrix} N\sigma_Y^2 Q & 0 \\ 0 & N\sigma_U^2 R \end{bmatrix} \right)^\dagger_\varepsilon L Y_T^\top (Y_T Y_T^\top - N\sigma_{Y_T}^2 I)^\dagger y_f \\ &= P_2 (P_1 - \sigma_{Y_T}^2 I)^\dagger y_f - (P_3 - P_2 (P_1 - \sigma_{Y_T}^2 I)^\dagger P_4) \cdot \\ &\quad \cdot \left(P_4^\top (P_1 - \sigma_{Y_T}^2 I)^\dagger P_4 + P_5 - \begin{bmatrix} \sigma_Y^2 Q & 0 \\ 0 & \sigma_U^2 R \end{bmatrix} \right)^\dagger_\varepsilon P_4^\top (P_1 - \sigma_{Y_T}^2 I)^\dagger y_f \end{aligned} \quad (28)$$

where $P_1 = \frac{1}{N} Y_T Y_T^\top$, $P_2 = \frac{1}{N} U_{0:T-1} Y_T^\top$, $P_3 = \frac{1}{N} U_{0:T-1} L^\top$, $P_4 = \frac{1}{N} Y_T L^\top$, and $P_5 = \frac{1}{N} L L^\top$. By the Strong Law of Large Numbers [7] and the assumption on the noise, as $N \rightarrow \infty$, it follows that

$$\begin{aligned} P_1 &= \frac{1}{N} Y_T Y_T^\top \xrightarrow{\text{a.s.}} \frac{1}{N} \bar{Y}_T \bar{Y}_T^\top + \sigma_{Y_T}^2 I =: \bar{P}_1, \\ P_2 &= \frac{1}{N} U_{0:T-1} Y_T^\top \xrightarrow{\text{a.s.}} \frac{1}{N} \bar{U}_{0:T-1} \bar{Y}_T^\top =: \bar{P}_2, \\ P_3 &= \frac{1}{N} U_{0:T-1} L^\top \xrightarrow{\text{a.s.}} \frac{1}{N} \bar{U}_{0:T-1} \left[\bar{Y}_{1:T-1}^\top Q^{1/2} \quad \bar{U}_{0:T-1}^\top R^{1/2} \right] =: \bar{P}_3, \\ P_4 &= \frac{1}{N} Y_T L^\top \xrightarrow{\text{a.s.}} \frac{1}{N} \bar{Y}_T \left[\bar{Y}_{1:T-1}^\top Q^{1/2} \quad \bar{U}_{0:T-1}^\top R^{1/2} \right] =: \bar{P}_4, \\ P_5 &= \frac{1}{N} L L^\top \xrightarrow{\text{a.s.}} \begin{bmatrix} \frac{1}{N} Q^{1/2} \bar{Y}_{1:T-1} \bar{Y}_{1:T-1}^\top Q^{1/2} + \sigma_Y^2 Q & \frac{1}{N} Q^{1/2} \bar{Y}_{1:T-1} \bar{U}_{0:T-1}^\top R^{1/2} \\ \frac{1}{N} R^{1/2} \bar{U}_{0:T-1} \bar{Y}_{1:T-1}^\top Q^{1/2} & \frac{1}{N} R^{1/2} \bar{U}_{0:T-1} \bar{U}_{0:T-1}^\top R^{1/2} + \sigma_U^2 R \end{bmatrix} =: \bar{P}_5. \end{aligned} \quad (29)$$

Notice that $\hat{u}_{0:T-1}^{(c)}$ is a continuous function of P_i around $P_i = \bar{P}_i$ for $i = 1, \dots, 5$ and $\varepsilon > 0$ sufficiently small. In light of this fact, (27) follows by using (29) and the Continuous Mapping Theorem [7, Theorem 2.3]. \square

Following the same argument as above, it is possible to establish asymptotically correct data-driven expressions of minimum-energy controls ($Q = 0$, $R = I$). Specifically, the

corrected version of (8) reads as

$$\hat{u}_{0:T-1}^{(c)} = (I - U_{0:T-1} \tilde{\Pi}_{Y_T} (U_{0:T-1} \tilde{\Pi}_{Y_T} U_{0:T-1}^\top - N \sigma_U^2 I)^\dagger_\epsilon) U_{0:T-1} (Y_T Y_T^\top - N \sigma_{Y_T}^2 I)^\dagger y_f, \quad (30)$$

whereas the corrected version of the compact data-driven control in (13) is

$$\hat{u}_{0:T-1}^{(c)} = (Y_T U_{0:T-1}^\top (U_{0:T-1} U_{0:T-1}^\top - N \sigma_U^2 I)^\dagger)^\dagger y_f. \quad (31)$$

Finally, the corrected approximate minimum-energy control in (14) reads as

$$\hat{u}_{0:T-1}^{(c)} = U_{0:T-1} (Y_T Y_T^\top - N \sigma_{Y_T}^2 I)^\dagger y_f. \quad (32)$$

It is worth noting that, while (30) requires correction terms for both input and output noises, (31) and (32) include correction terms only for one source of noise (input noise in (31) and output noise in (32)). In particular, if the noise corrupts output data only, (31) coincides with the original data-driven control in (13).

SUPPLEMENTARY REFERENCES

- [1] Kailath, T. *Linear Systems* (Prentice-Hall, 1980).
- [2] Ben-Israel, A. & Greville, T. N. E. *Generalized inverses: theory and applications*, vol. 15 of *CMS Books in Mathematics* (Springer-Verlag New York, 2003), 2nd edn.
- [3] Vershynin, R. *Introduction to the non-asymptotic analysis of random matrices*, 210–268 (Cambridge University Press, 2012).
- [4] Searle, S. R. *Matrix algebra useful for statistics* (John Wiley & Sons, 1982).
- [5] Pasqualetti, F., Zampieri, S. & Bullo, F. Controllability metrics, limitations and algorithms for complex networks. *IEEE Transactions on Control of Network Systems* **1**, 40–52 (2014).
- [6] Dean, S., Mania, H., Matni, N., Recht, B. & Tu, S. On the sample complexity of the linear quadratic regulator. *Foundations of Computational Mathematics* 1–47 (2019).
- [7] Van der Vaart, A. W. *Asymptotic statistics*, vol. 3 of *Cambridge Series in Statistical and Probabilistic Mathematics* (Cambridge University Press, 2000).